Flow-induced noise regimes of a three-dimensional airfoil

Danielle Moreau

School of Mechanical and Manufacturing Engineering, UNSW Sydney, Australia

ABSTRACT

The flow-induced noise produced by a surface-mounted three-dimensional (or finite length) airfoil is important for many aerodynamic and hydrodynamic applications. Examples include wing-fuselage junctions, turbomachinery blade, rotor tip and end-wall flows, and ship appendage and hull-junction flows. This presentation provides an overview of the three-dimensional airfoil noise program at UNSW Sydney. In general, there are four flow regimes for a three-dimensional airfoil. These are the airfoil-wall junction flow featuring a horseshoe vortex that wraps around the airfoil base; turbulent flow interaction with the leading edge; trailing edge flow whose structure depends upon the Reynolds number; and the tip flow that consists of vortices that form as the flow wraps around the free-end of the airfoil. The acoustic signature and turbulent noise sources associated with each of these flow regimes will be examined using anechoic wind tunnel measurements obtained with acoustic array, unsteady surface pressure and turbulence measurement methods.

1 INTRODUCTION

Airfoils are employed in many noise sensitive applications and as such, flow-induced airfoil noise is a much studied topic. Most studies on airfoil noise focus on the leading or trailing edge noise generated by a two-dimensional or semi-infinite airfoil. However, in practice, real-world technologies employ airfoils that are wall-mounted and finite in length such as wind turbine blades attached to a hub, submarine hydrofoils mounted to a hull or stators connected to a hub or outer wall. The flow field around a wall-mounted finite airfoil is complex and features several three-dimensional fluid phenomena due to end effects, as shown in Fig. 1. In the lower boundary layer, a horseshoe vortex system is present around the airfoil base and extends into the wake. Vortex structures may also form at the tip of the finite airfoil, convect downstream of the airfoil trailing edge and eventually form a trailing vortex. These tip and junction vortex structures may form depending on the airfoil aspect ratio (length to chord ratio L/C) and the airfoil length to thickness ratio, L/T, which influences how much flow goes over the tip of the airfoil instead of around it. Other factors that influence the flow field around the airfoil include the airfoil profile and tip shape, Reynolds number, angle of attack, the incoming boundary layer thickness, the free-stream turbulence level and the roughness of the wall and airfoil surface.

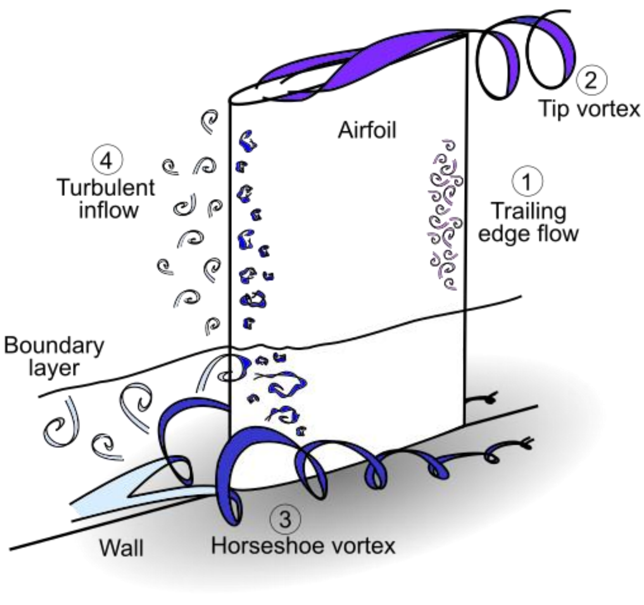

Figure 1: Flow-induced noise mechanisms of a wall-mounted finite length airfoil.

The purpose of this paper is to review the aeroacoustic source mechanisms of a three-dimensional airfoil associated with the 4 major flow regimes illustrated in Fig. 1: (1) trailing edge noise, (2) tip vortex formation noise, (3) junction noise and (4) leading edge (or airfoil-turbulence interaction) noise. Some current research results obtained from our on-going experimental program on these different noise mechanisms are reviewed and presented. The aim of this paper is to inform the acoustics community of the physics controlling the flow-induced noise of a wall-mounted finite airfoil along with our plans for future research.

2 METHODOLOGY

Table 1 provides a summary of the different experimental campaigns that have been performed to examine the flow noise produced by a wall-mounted finite airfoil as part of this on-going study. The test case considered is an airfoil mounted to a wall (either the wind tunnel wall/ceiling or a side plate attached to the wind tunnel outlet). Experiments have been performed in five different wind tunnel facilities at four institutions. Table 1 states the wind tunnel facility in which tests were performed, the airfoil aspect ratio (L/C), ratio of incoming boundary layer thickness to airfoil span (δ/L), chord-based Reynolds number (Re_C) and the geometric angle of attack (α). Also stated in Table 1 are the different flow and noise measurement techniques employed in each facility. Images of two experimental campaigns are provided in Fig. 2. Readers are directed to the relevant studies referenced in Table 1 for full descriptions of the different experimental methodologies. The measurements obtained in the different campaigns will be used in the following sections to examine the different aeroacoustic source mechanisms of a wall-mounted finite airfoil.

Table 1: A summary of wall-mounted finite airfoil noise experimental campaigns. PIV refers to particle image velocimetry.

Facility	L/C	δ/L	Re_C	$\alpha,^\circ$	NACA profile	Measurement techniques
U. of Adelaide (UA) anechoic wind tunnel[1]	0.2 – 2	0.078 – 0.88	9.2e4 – 1.6e5	0 – 10	0012	Two perpendicular 31 microphone arrays, hot-wire anemometry
Virginia Tech (VT) Stability Wind Tunnel[2]	1, 2, 3	0.061 – 0.18	7.9e5 – 1.6e6	0 – 12	0012	117 microphone array, wake pressure rake
UNSW acoustic tunnel (UAT) and large aerodynamic tunnel[3]	0.2 – 2	0.035 – 0.35	4.6e4 – 2.3e5	0 – 20	0012 – 0018 2412 – 6412	64 microphone array, remote microphone surface pressure technique, hot-wire anemometry, Cobra and pitot probes, PIV
Brandenburg Technical U. (BTU) aeroacoustic wind tunnel[4]	2	0.034 – 0.067	4.6e4 – 2.3e5	0 – 20	0012 – 0018 2412 – 6412	47 microphone array, hot-wire anemometry

[1] Moreau et al. (2014).
[2] Moreau and Doolan (2016a); Moreau and Doolan (2016b); Moreau et al. (2016).
[3] Awasthi et al. (2018); Awasthi et al. (2020); Ding et al. (2020); Ding et al. (2021).
[4] Ding et al. (2021); Geyer and Moreau (2021); Geyer et al. (2020); Moreau et al. (2018); Schneehagen et al. (2021); Zhang et al. (2020a); Zhang et al. (2020b); Zhang et al. (2021).

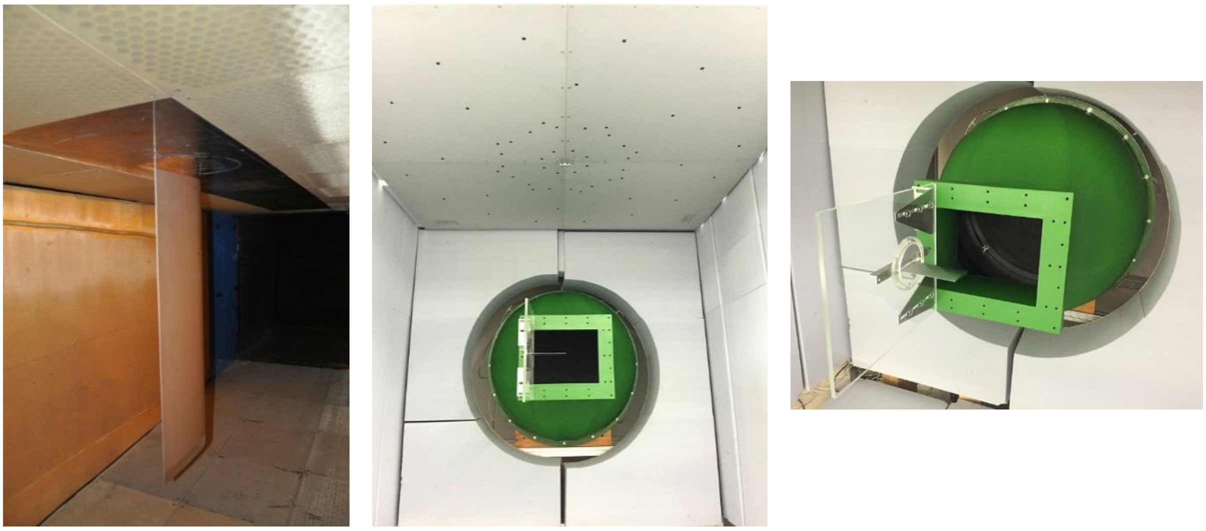

(a) (b) (c)

Figure 2: Wall-mounted finite airfoil experimental campaigns performed in (a) the VT Stability Wind Tunnel and (b), (c) the BTU aeroacoustic wind tunnel. In (a), an airfoil with $L/C = 3$ is mounted to the ceiling in the kevlar walled aeroacoustic test section. The acoustic array is in an anechoic chamber located on the other side of the kevlar wall. In (b), (c), an airfoil with $L/C = 2$ is mounted to a side plate attached to a rectangular nozzle. The acoustic array can be seen in (b) in the ceiling of the anechoic chamber surrounding the nozzle.

3 NOISE SOURCE CONTRIBUTION OF DIFFERENT FLOW REGIMES

Figure 3 presents spectral data that shows the contribution of individual noise sources for a wall-mounted finite airfoil associated with the four flow regimes illustrated in Fig. 1. These measurements, documented in Moreau et al. (2016), were obtained for a NACA0012 airfoil with $L/C = 3$ at $Re_C = 1.6e6$. The airfoil surface was artificially tripped, ensuring that the boundary layers are in a turbulent flow state at the trailing edge leading to the production of broadband trailing edge noise. A microphone array was used to produce sound maps that display the location and strength of the different airfoil noise sources. Acoustic spectra were then estimated by integrating the sound maps over different regions of interest. The integration regions were selected to allow estimation of the complete airfoil noise spectrum and individual contributions from the trailing edge (TE), leading edge (LE), junction, and tip (please see Moreau et al. (2016) for definition of the integration regions). It is important to note that the trailing edge and leading edge regions encompass the entire airfoil span and thus include some contribution from the junction and tip. In Fig. 3, the x axis indicates both frequency in kHz and Strouhal number based on airfoil chord, St_C.

Figure 3 shows that junction noise is the dominant airfoil noise mechanism at low frequencies (below $St_C = 10$). Inspection of the beamforming sound maps determined that the junction noise source is localised on the airfoil leading edge. This indicates that the low frequency noise mechanism is the interaction of the horseshoe vortex (and associated separated flow region) with the airfoil leading edge. In the mid frequency range ($St_C = 10 - 20$), the trailing edge is the significant source of noise at low angles of attack. Relative to the end sources (tip and wall-junction noise), trailing edge noise becomes less significant as the angle of attack is increased. At a high angle of attack of $\alpha = 12°$, the dominant noise sources are located at the leading edge–wall junction and the airfoil trailing edge–tip (see Fig. 3 (b)). Each of these individual noise sources will be discussed separately in the following sections.

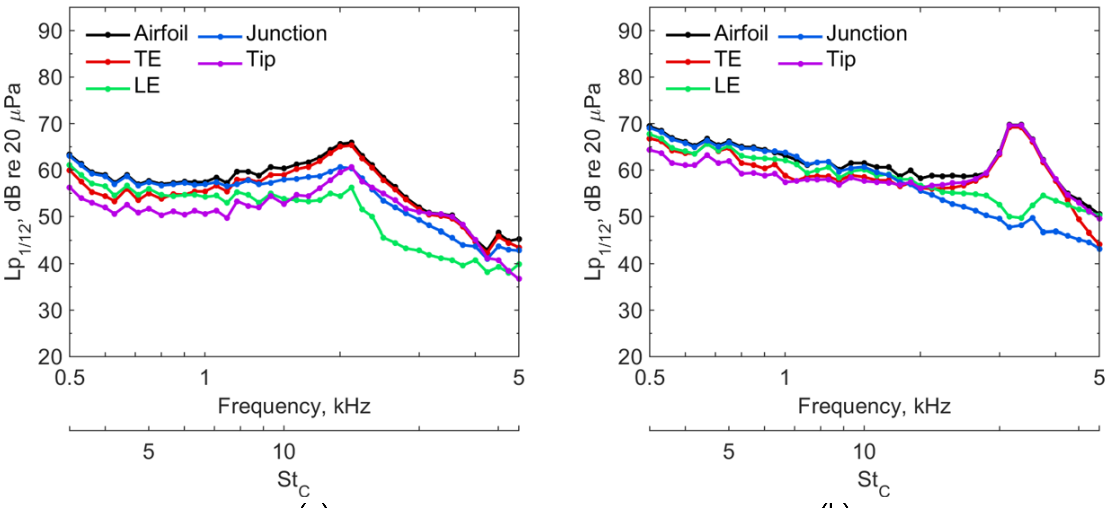

Source: Moreau et al. (2016)

Figure 3: 1/2th octave band airfoil, trailing edge, leading edge, junction, and tip spectra for a NACA0012 airfoil with $L/C = 3$ at $Re_C = 1.6e6$. (a) $\alpha = 0°$ and (b) $\alpha = 12°$.

4 TRAILING EDGE NOISE

Trailing edge noise can be categorised as tonal or broadband. Tonal noise is produced in a laminar-transitional boundary layer flow regime or when blunt trailing edge vortex shedding occurs. Broadband noise is generated when turbulent boundary layers form on the surface of the airfoil and interact with the sharp trailing edge. While a large body of literature exists describing studies on the production and prediction of airfoil trailing edge noise, these have focused on two-dimensional or semi-infinite airfoils (e.g. Brooks et al., 1989). In the case of a wall-mounted finite airfoil, the three-dimensional tip and junction flows interact with the mid-span flow to alter the flow field at the trailing edge across the airfoil span. Subsequently, the presence of end effects will impact the generation of trailing edge noise.

To illustrate the impact of junction and tip flows on the trailing edge flow field, Fig. 4 shows spanwise mean velocity profiles measured along the trailing edge (in the spanwise y direction) of a NACA0012 airfoil with $L/C = 0.5$ at $\alpha = 0°$ and $Re_C = 2.74e5$ (Awasthi et al., 2018). Within these profiles, 4 distinct trailing edge flow regions exist due to end effects. In the near wall region (1), the velocity rises as we move away from the wall due to the influence of the junction flow which is largely confined to a region with height equal to that of the incoming wall boundary layer. In region (2), the velocity field at the trailing edge is two-dimensional, and the mean velocity does not vary much across the span. Close to the airfoil, a region of spanwise shear (region 3), with a local velocity minimum is observed as we approach the tip. In region (4), the presence of the tip vortex is observed to create a large velocity deficit. The results have been shown here at non-lifting conditions; the change in spanwise flow organisation becomes even more pronounced at non-zero angle of attack and the two-dimensional flow region further reduces in size. Understanding how airfoil three-dimensionality affects trailing edge noise production and prediction has thus been a significant focus of our research.

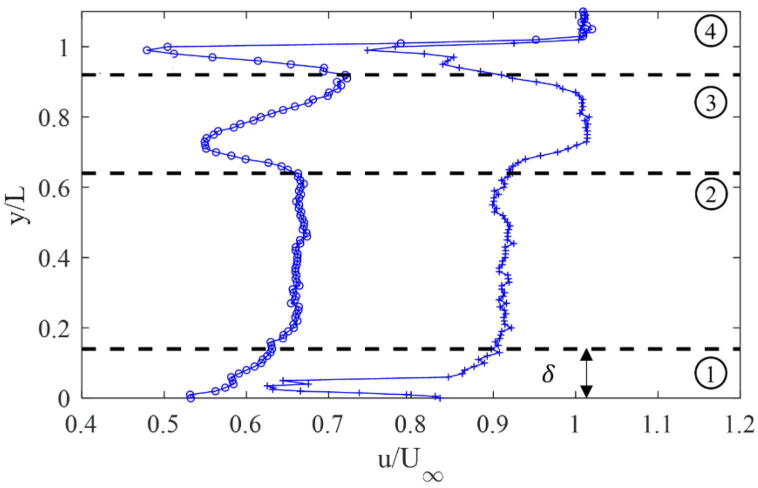

Source: Awasthi et al. (2018)

Figure 4: Spanwise mean velocity profiles measured along the trailing edge of a NACA0012 airfoil with $L/C = 0.5$ at $Re_C = 2.74e5$ and $\alpha = 0°$ at 5 mm downstream of the trailing edge (o) and 180 mm downstream of the trailing edge (+).

Considering tip flow effects, a semi-empirical prediction method has been developed for the turbulent boundary layer trailing edge noise produced by a wall-mounted finite length NACA0012 airfoil with flat tip (Moreau et al., 2016). An example of the turbulent boundary layer trailing edge noise spectrum is given in Fig. 3. The prediction method employs the Brooks, Pope, and Marcolini (Brooks et al., 1989) trailing edge noise model (referred to as the BPM model) modified to incorporate spanwise variations in airfoil flow properties in combination with the BPM flat tip noise model. First, Prandtl's classical lifting-line theory (Katz and Plotkin, 2001) for a rectangular planform wing is used to obtain the spanwise circulation and effective angle of attack distribution of the wall-mounted finite airfoil. As an example, the spanwise effective angle of attack distribution (α_e) for a NACA0012 airfoil with $L/C = 0.5$ is shown in Fig. 5. In this figure, the effective angle of attack distribution measured using a four-hole Cobra pressure probe is compared with Prandtl's lifting-line theory. Good comparison is achieved in the mid-span and tip region. It can be observed that the tip flow field has influence over the entire airfoil span, significantly reducing the effective angle of attack especially in the region immediately inboard of the tip. The tip vortex changes the effective angle of attack by influencing the oncoming flow towards the leading edge where downwash reduces the local angle of attack. The airfoil span is then discretized into small segments, and XFOIL is used to determine the aerodynamic properties of each segment. The trailing edge noise prediction for each segment is then calculated using the BPM turbulent boundary layer trailing edge noise model, and the tip noise was estimated with the BPM flat tip noise model. An example of the prediction obtained with this method (labelled BPM WMA TE & Tip) compared with noise measurements (labelled Exp. WMA TE) is given in Fig. 6. At zero angle of attack (Fig. 6 (a)), the wall-mounted finite airfoil trailing edge noise is well predicted across the entire frequency range. At high angles of attack (Fig. 6 (b)), the finite airfoil trailing edge noise prediction agrees well with the measured spectrum at $St_C < 18$. The BPM tip noise model underpredicts the peak level and frequency of trailing edge tip noise contributions at $St_C > 18$. To account for this underprediction, a new empirical flat tip noise model was proposed in Moreau et al. (2016) that provides a good estimate of experimental tip noise data to within a few dB.

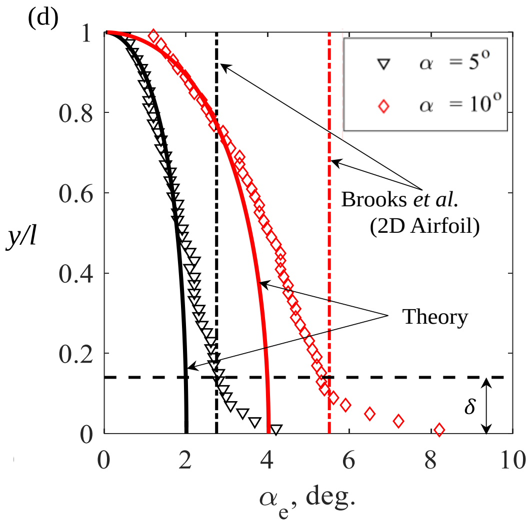

Source: Awasthi et al. (2018)
Figure 5: Measured spanwise effective angle of attack distribution α_e for a NACA0012 airfoil with $L/C = 0.5$ at $Re_C = 2.74e5$ (markers) compared with lifting line theory (solid lines).

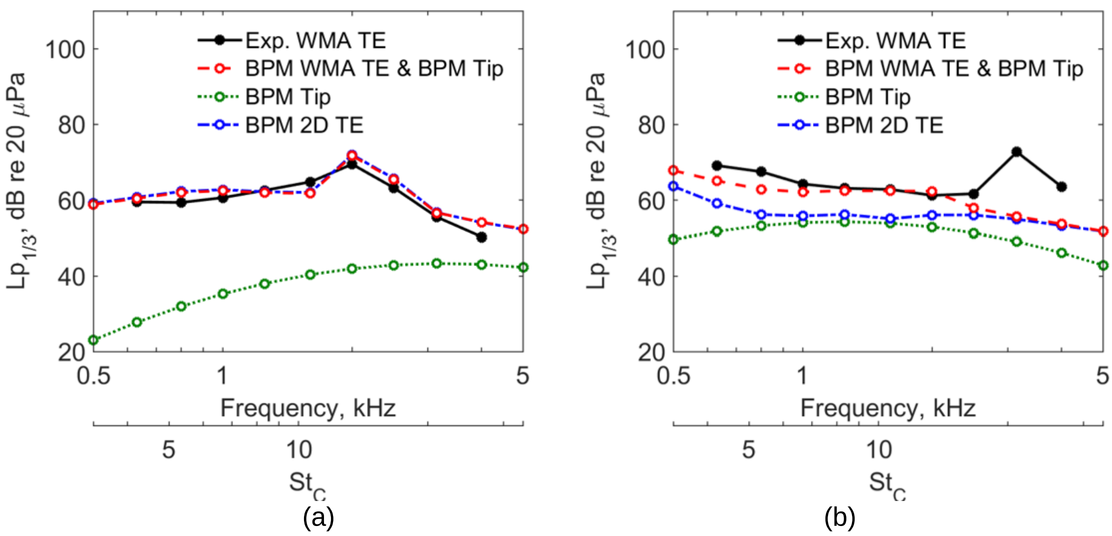

Source: Moreau et al. (2016c)
Figure 6: 1/3rd octave band trailing edge noise spectra for a NACA0012 airfoil with $L/C = 3$ at $Re_C = 1.6e6$ compared with the BPM Model. (a) $\alpha = 0°$ and (b) $\alpha = 12°$.

Airfoil three-dimensionality also affects the production of tonal trailing edge noise in a laminar-transitional boundary layer flow regime. Airfoil tonal noise is produced by an aeroacoustic feedback loop between flow instabilities (Tollmein-Schlicting waves) in the boundary layer and acoustic waves generated at the trailing edge (Arbey and Bataille, 1983). The feedback process acts as a discrete frequency selection mechanism by reinforcing only certain frequencies for which the acoustic and velocity disturbances are in phase at the first point of instability in the laminar boundary layer. These discrete frequencies are amplified in a separated flow region and then diffracted by the trailing edge, resulting in the production of tonal noise (Nash et al., 1999; Probsting and Yarusevych, 2015).

An example of the tonal noise produced by a NACA0012 airfoil with $L/C = 2$ at $Re_C = 2.3e5$ is given in Fig. 7 (a). In the case of a wall-mounted finite airfoil, flow features that form due to end effects introduce significant spanwise variation to the flow, altering the spanwise extent and position of flow separation near the trailing edge (Moreau and Doolan, 2016b). The laminar separation bubble and tonal noise source location have been shown to shift along the airfoil trailing edge towards the free-end region with increasing geometric angle of attack due to the influence of the tip flow field over the airfoil span. Compared to a two-dimensional airfoil, the domain of tonal noise production from a wall-mounted finite airfoil extends over a much larger range of Reynolds numbers and geometric angles of attack. As the airfoil aspect ratio is reduced, tonal noise production shifts to lower Reynolds numbers and spreads to higher geometric angles of attack.

Varying the camber and thickness of a wall-mounted finite airfoil also influences the operating conditions at which tonal noise production occurs (Moreau et al., 2018; Geyer and Moreau, 2021). This is illustrated in Fig. 7, which compares the tonal noise produced by a NACA0012 and NACA4412 airfoil with $L/C = 2$ and 0 and 4% camber respectively, at 40% chord. The NACA0012 produces a high amplitude primary tone accompanied by several weaker side tones at all angles of attack. At the same flow conditions, the NACA4412 produces a set of lower amplitude equispaced tones and tonal noise is even suppressed at high angles of attack. For a given angle of attack, increasing camber results in an increase in lift coefficient and a shift in tonal noise production to higher Reynolds numbers. This is illustrated in Fig. 7 (c), which shows envelopes that define the operating conditions for tonal production from airfoils with differing amounts of camber. Tonal noise production does not collapse with lift coefficient, demonstrating that the local flow conditions influence the noise source. Figure 7 (d) also compares the different tonal noise spectra produced by the NACA0012 and NACA4412 airfoils at the same lift coefficient. The local pressures on the airfoil surface are impacted by both finite span and camber effects, which alters the location of flow separation on the surface of the airfoil and subsequently, the tonal noise signature.

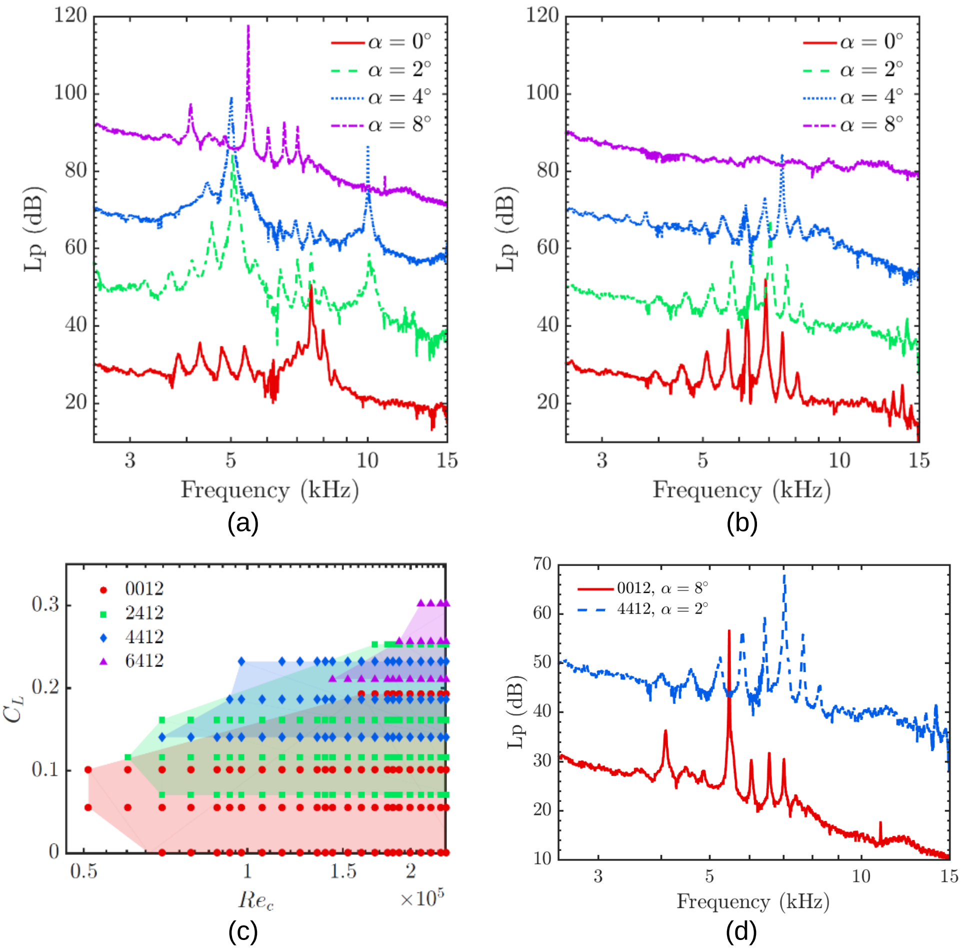

Source: Moreau et al. (2018)

Figure 7: Narrowband acoustic spectra for (a) NACA0012 and (b) NACA4412 airfoils with $L/C = 2$ at $Re_C = 2.3e5$. Spectra have been offset by 20 dB with each increase in angle of attack. (c) Tonal envelopes showing operating conditions for tonal noise production from airfoils with variation in camber. (d) Acoustic spectra for the NACA0012 and NACA4412 at $C_L = 0.19$. In the legend, ‘xx12’ refers to airfoil profile shape NACAxx12.

5 TIP VORTEX FORMATION NOISE

Tip vortices form at the free-end of a wall-mounted finite airfoil at both zero lift and lifting conditions. Under lifting conditions, the pressure difference between the suction and pressure sides of the airfoil drives cross-flow over the tip surface leading to formation of a tip vortex. Meanwhile at zero lift, non-parallel flow effects between the free-stream flow and the flow over the airfoil surface leads to the production of two vortices of opposite signs on either side of the airfoil (Giuni and Green, 2013). Noise generation is associated with the passage of highly turbulent flow over the tip and trailing edge. Figure 8 (a) shows an example of the tip noise spectra produced by a NACA0012 airfoil with flat tip at various Reynolds numbers ($U_\infty = 30 - 60$ m/s corresponding to $Re_C = 7.9e5 - 1.6e6$) and geometric angles of attack ($\alpha = 0° - 12°$) (Moreau and Doolan, 2016a). To illustrate the tip vortex that is produced by the airfoil at $\alpha = 12°$, Fig. 8 (b) shows a plane of mean velocity measured in the spanwise (y), wall-normal (z) direction at 8.4 chord lengths downstream of the trailing edge. The airfoil trailing edge can be identified as the thin central contour region with slight velocity deficit and the tip vortex can be observed at y = -0.2 m which corresponds to the position of the trailing edge tip corner. As shown in Fig. 8 (and Fig. 3), the tip noise spectrum exhibits a broad peak (i.e centred on 4.2 kHz at $U_\infty = 60$ m/s). The tip noise peak increases in amplitude as the angle of attack and to a lesser extent, flow speed, is increased. The frequency of the tip noise peak is also observed to reduce as flow speed is decreased. The amplitude of the tip noise peak in Fig. 8 scales with Mach number $M^{7.5}$ at each angle of attack. This is higher than the well-known edge-scattering scaling of M^5 for trailing edge noise. Mathias et al. (1998) also reported a similar Mach number dependence of M^8 when scaling the tip noise data of Brooks and Marcolini (1986).

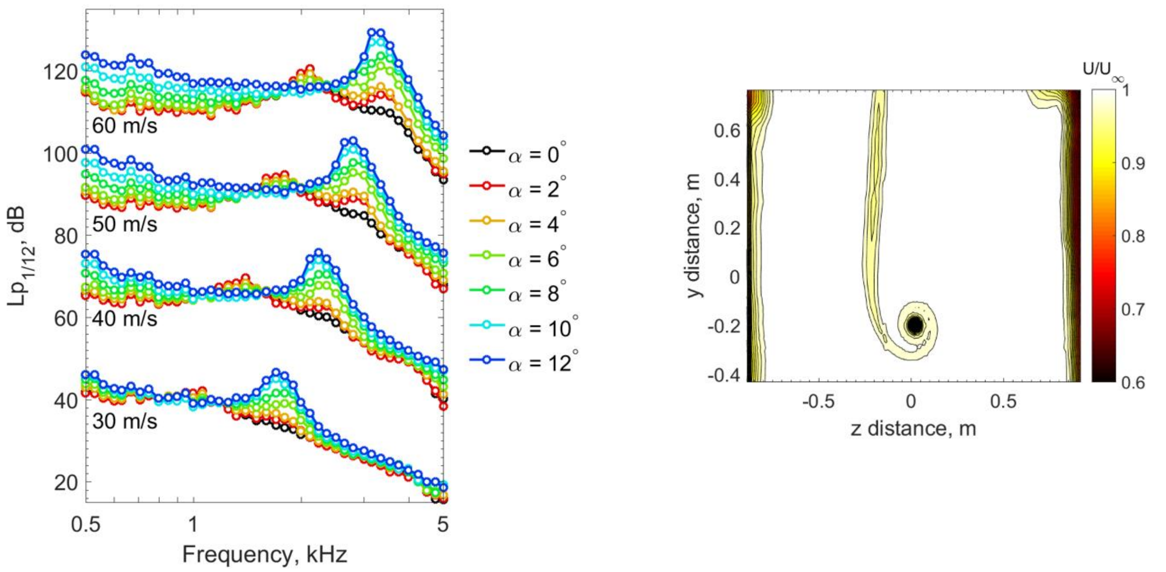

(a) (b)

Source: Moreau and Doolan (2016a)

Figure 8: (a) 1/2th octave band tip noise spectra for a NACA0012 airfoil with $L/C = 3$ at $Re_C = 7.9e5 - 1.6e6$. Note that with each increase in flow speed, the spectra have been offset by 20 dB for clarity. (b) Normalised mean velocity contours in the airfoil wake at 8.4 chord lengths downstream of the airfoil trailing edge at $\alpha = 12°$ and $Re_C = 1.6e6$. The flow direction is out of the page.

As shown by Buffo et al. (2012), the shape of the airfoil tip influences both the tip vortex topology (its strength and position relative to the wing surface) and its axial velocity components. It follows that the airfoil profile and tip shape will impact the tip noise signature. To illustrate this, Fig. 9 shows the tip noise spectra of airfoils with variations in thickness (12, 15 and 18% of chord) and tip shape (NACA0012 with a flat and rounded tip). As shown in Zhang et al. (2021), a critical frequency exists to delimitate thickness effects on the tip noise spectra, which increases with Reynolds number and remains fairly constant with angle of attack (see Fig. 9 (a) and (b)). The thinnest airfoil (NACA0012) produces the lowest noise levels below the critical frequency (e.g. 3 kHz at $Re_C = 1.5e5$ in Fig. 9 (a)), meanwhile above the critical frequency, it generates the highest amplitude tip noise peak. In general, the NACA0018 has the lowest tip noise levels, especially at mid-to-high frequencies above 5 kHz. Rounding the airfoil tip can reduce the tip noise level by more than 5 dB over the frequency range from 3 to 12 kHz (see

Fig. 9 (c) and (d)). The exact flow mechanism responsible for changes in noise generation with geometrical variations is the subject of on-going investigation.

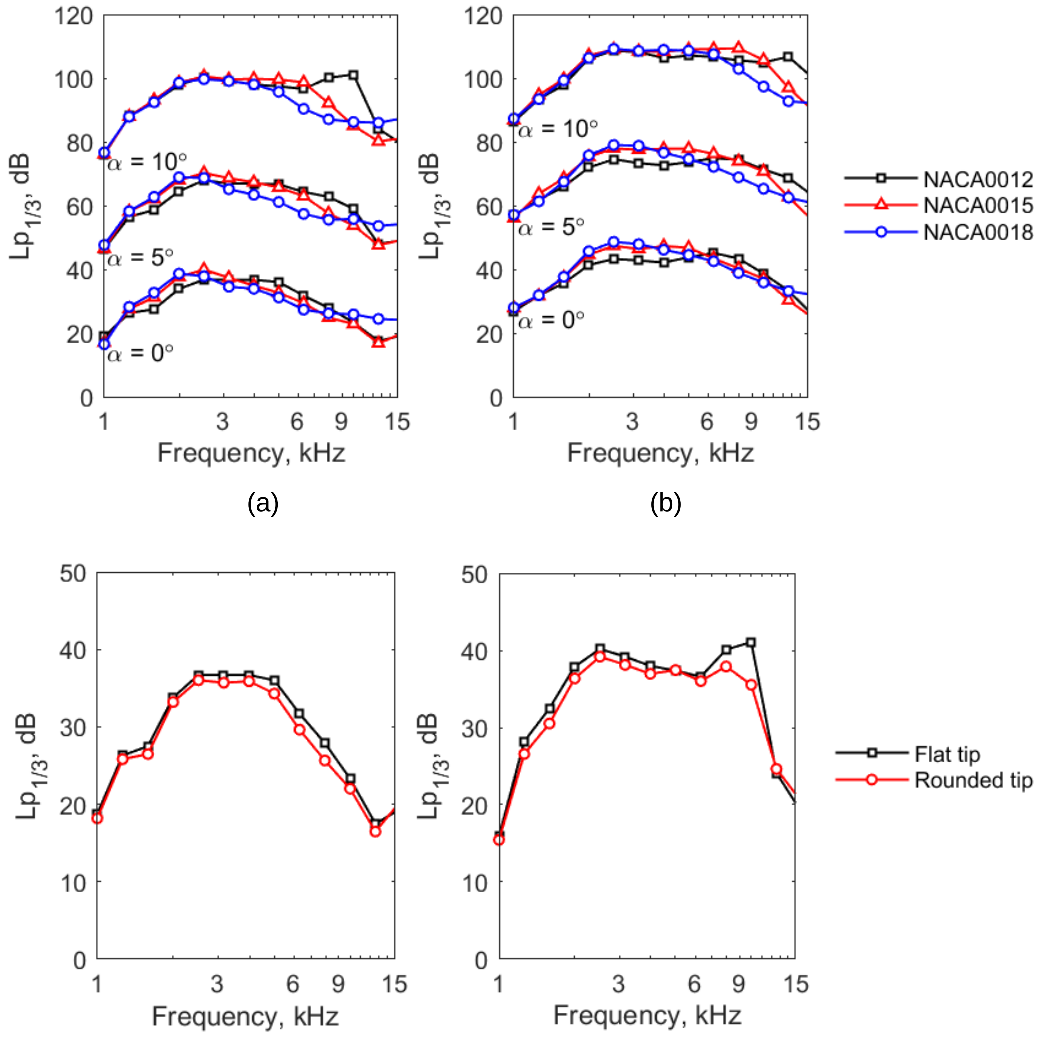

(a) (b)

(c) (d)

Source: Zhang et al. (2021)

Figure 9: 1/3rd octave band tip noise spectra for airfoils with $L/C = 2$ and geometric variations. Symmetric airfoils with varying thickness and a flat tip at a range of angles of attack and Reynolds numbers of (a) $Re_C = 1.5e5$ and (b) $Re_C = 2.25e5$. NACA0012 airfoil with flat and rounded tips at $Re_C = 1.5e5$ and angles of attack of (c) $\alpha = 0°$ and (d) $\alpha = 10°$. In (a) and (b), spectra at $\alpha = 5°$ and 10° have been offset by 30 and 60 dB, respectively.

Our recent work on tip noise involves the development of novel tip devices for noise control that include serrations, porosity (Geyer et al., 2020; Zhang et al., 2020b) and end plates (Schneehagen et al., 2020). Fig. 10 shows an example of the noise attenuation capability of the porous tip devices. The porous tips were created by 3D-printing the flat tip portion of the airfoil with small circular perforations (holes) and these were then mounted to an aluminum base wing. Compared to a solid flat tip, the porous tips produce a noise reduction at low frequencies (below 3 kHz) on the order of 2 to 3 dB. However, a high frequency noise increase is also observed that increases with the diameter of the pores suggesting it is a roughness noise contribution.

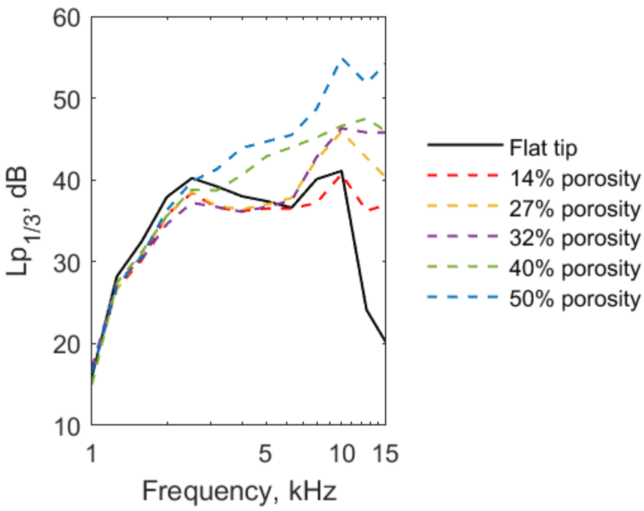

Figure 10: 1/3rd octave band spectra obtained with porous tips on a tripped NACA0012 airfoil with $L/C = 2$ at $\alpha = 10°$ and $Re_C = 1.5e5$.

6 WING-IN-JUNCTION SURFACE PRESSURE MEASUREMENTS

At the airfoil-wall junction, a horseshoe vortex forms at the airfoil leading edge with streamwise legs of opposite rotational sense that stretch around the airfoil base and convect downstream. This vortical flow structure forms due to the large adverse pressure gradients created by the airfoil that cause the incoming boundary layer to separate and then roll up around itself (Simpson, 2001). The turbulence generated by the boundary layer separation and the unsteady horseshoe vortex structure can enhance unsteady surface loading in the airfoil-wall junction region and lead to far-field noise radiation (as observed in Fig. 3). To understand the nature of airfoil-wall junction flows, detailed mean and fluctuating wall pressure measurements in the vicinity of the junction region have been obtained (Ding et al., 2020; Awasthi et al., 2020) and some highlights of this work are presented here. In particular, we have focused on aspect ratio and angle of attack effects on the wall pressure field.

Figure 11 shows measurements of the mean pressure field in the junction region around a NACA0012 airfoil at $Re_C = 8.7e4$ and various angles of attack (Ding et al., 2020). These measurements have been obtained using a detailed array of pressure taps located in the wall around the airfoil (see Fig. 11 (e)). The wall pressure maps show complex details of the mean flow structure and its variation with angle of attack. At zero angle of attack, the flow field is symmetric (Fig. 11 (a)). Increasing the angle of attack (in Fig. 11 (b) – (d)) results in the formation of a low-pressure region downstream of the leading edge on the suction side of the airfoil. There is also downward movement of the leading edge high pressure region on the pressure side with increasing angle of attack.

Figure 12 shows the RMS fluctuating pressure coefficient measured on the wall around the suction side of a NACA0012 airfoil with various aspect ratios at $Re_C = 2.74e5$ and two angles of attack (Awasthi et al., 2020). Both the airfoil aspect ratio and angle of attack are observed to influence the RMS pressure levels around the wing. In all cases, the fluctuating pressure is highest upstream of the leading edge due to the presence of flow separation and the formation of the horseshoe vortex. The RMS pressure levels are higher at all streamwise locations at the higher angle of attack (in Fig. 12 (b)). This rise is most pronounced for the $L/C = 1$ case especially past the maximum thickness location. A noticeable increase in the fluctuating pressure is also observed downstream of the trailing edge.

Figure 13 shows the wall pressure spectra measured around the NACA0012 airfoil with various aspect ratios at $Re_C = 2.74e5$ and two angles of attack (Awasthi et al., 2020). The spectra have been obtained upstream of the leading edge ($x/c = -0.025$), at two locations on the suction side of the airfoil ($x/c = 0.275, 0.8$) and at the trailing edge ($x/c = 0.98$) and are also compared to the undisturbed boundary layer spectrum at each location. In Fig. 13, the spectral density is normalized on the freestream dynamic pressure and boundary layer thickness, while the frequency is normalized on the boundary layer thickness and freestream velocity. Considering first the upstream measurement location, a considerable increase in the low frequency energy content is observed in the junction region compared to the undisturbed spectrum at zero angle of attack. Here, aspect ratio only impacts the pressure fluctuation levels at low frequencies. At the higher angle of attack, increases in the magnitude of the wall pressure fluctuations over the entire frequency range are observed. On the suction side of the airfoil, the spectra are similar for the $L/C = 0.2$ and 0.5 cases, while the spectra for $L/C = 1$ show higher levels. Downstream of the trailing edge, the spectral shape differs to that measured upstream with lifting conditions introducing a considerable aspect ratio effect.

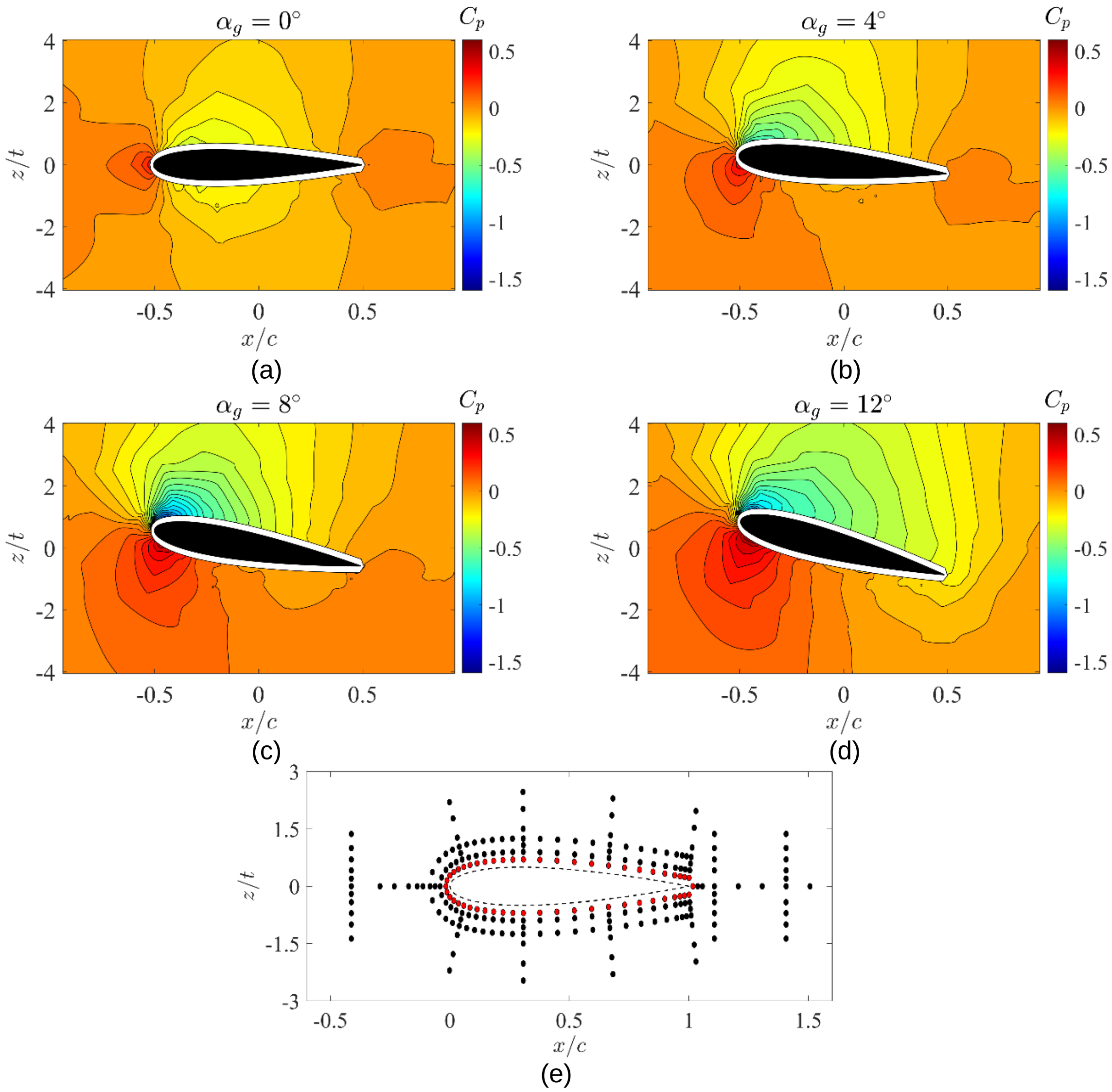

Source: Ding et al. (2020)

Figure 11: Contour maps of the mean wall pressure coefficient distribution for a NACA0012 airfoil with $L/C = 2$ at $Re_C = 8.7e4$ and (a) $\alpha = 0°$, (b) $\alpha = 4°$, (c) $\alpha = 8°$ and (d) $\alpha = 12°$. The pressure tap locations on the wall around the airfoil are shown in red and black in (e). The flow is from left to right and the airfoil is shown as a black dashed line.

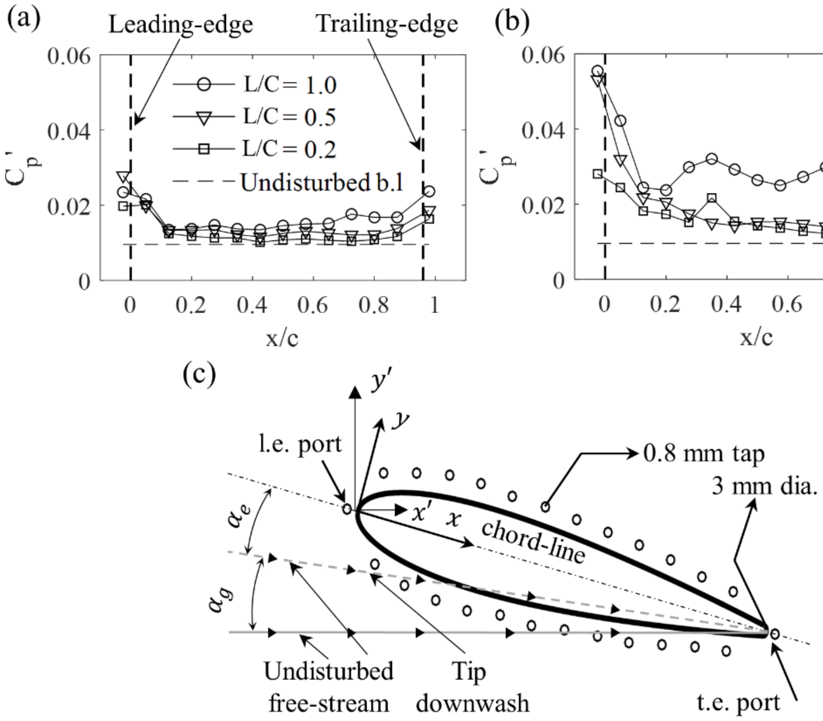

Source: Awasthi et al. (2020)

Figure 12: RMS fluctuating pressure coefficient on the wall around a NACA0012 airfoil on the suction side at $Re_C = 2.74e5$ and (a) $\alpha = 0°$, (b) $\alpha = 10°$. The pressure tap locations on the wall around the airfoil are shown in (c). Undisturbed b.l. refers to the RMS pressure on the plate without the presence of the airfoil. The dashed vertical lines refer to the airfoil leading and trailing edge and the flow is from left to right.

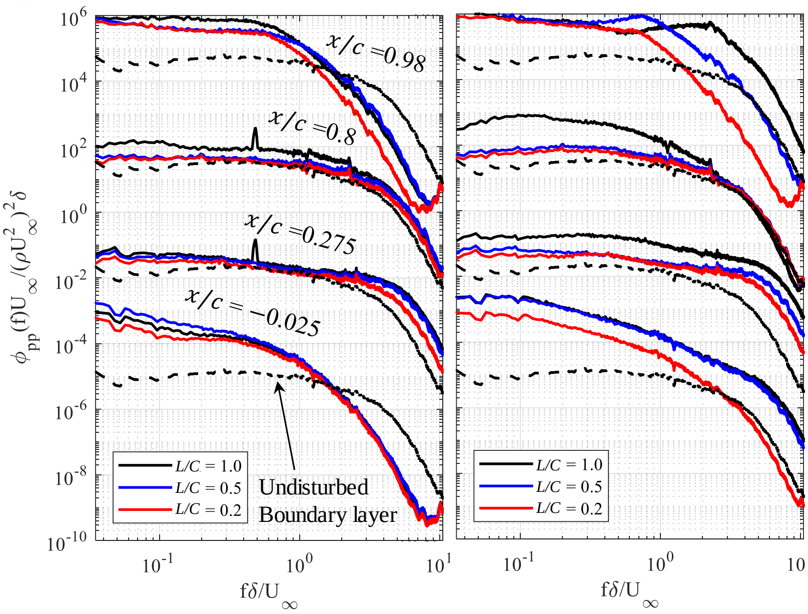

(a) (b)

Source: Awasthi et al. (2020)

Figure 13: Normalised surface pressure spectra on the airfoil suction side at $Re_C = 2.74e5$ and (a) $\alpha = 0°$ and (b) $\alpha = 10°$. The pressure tap locations on the wall around the airfoil are shown in Fig. 12 (c). Each set of spectra has been offset by 32 dB for clarity.

7 LEADING EDGE NOISE

Our future research focus is the fourth and final airfoil noise mechanism: leading edge or airfoil-turbulence interaction noise created whenever turbulent flow encounters an airfoil. Our aim is to understand how complex turbulent in-flows affect airfoil leading edge noise production. To do this, we have constructed a novel, turbulence and boundary layer-airfoil interaction experiment in the UAT. It allows airfoils to be immersed in homogenous, isotropic turbulence and anisotropic turbulent boundary layers under controlled conditions. A conceptualised sketch of the experiment is shown in Fig. 14. To first examine airfoil noise generation in homogenous, isotropic turbulence, a grid will be placed upstream of the contraction outlet. Following this, we will examine the noise of a finite airfoil partially and fully immersed in a thickened zero pressure gradient and pressure gradient turbulent boundary layers. To study the effect of pressure gradient, the end-wall flap deflection angle will be modified. By varying the ramp angle, a variety of favourable and adverse pressure gradients will be produced and by doing so we will introduce non-homogeneous and non-isotropic turbulence effects in a controlled manner. This experiment will allow us to relate the fine details of complex turbulent in-flow (characterised using PIV measurements) to the airfoil surface pressure response (using surface pressure taps) and far-field noise (measured using an acoustic array), providing insight into finite airfoil leading edge noise production.

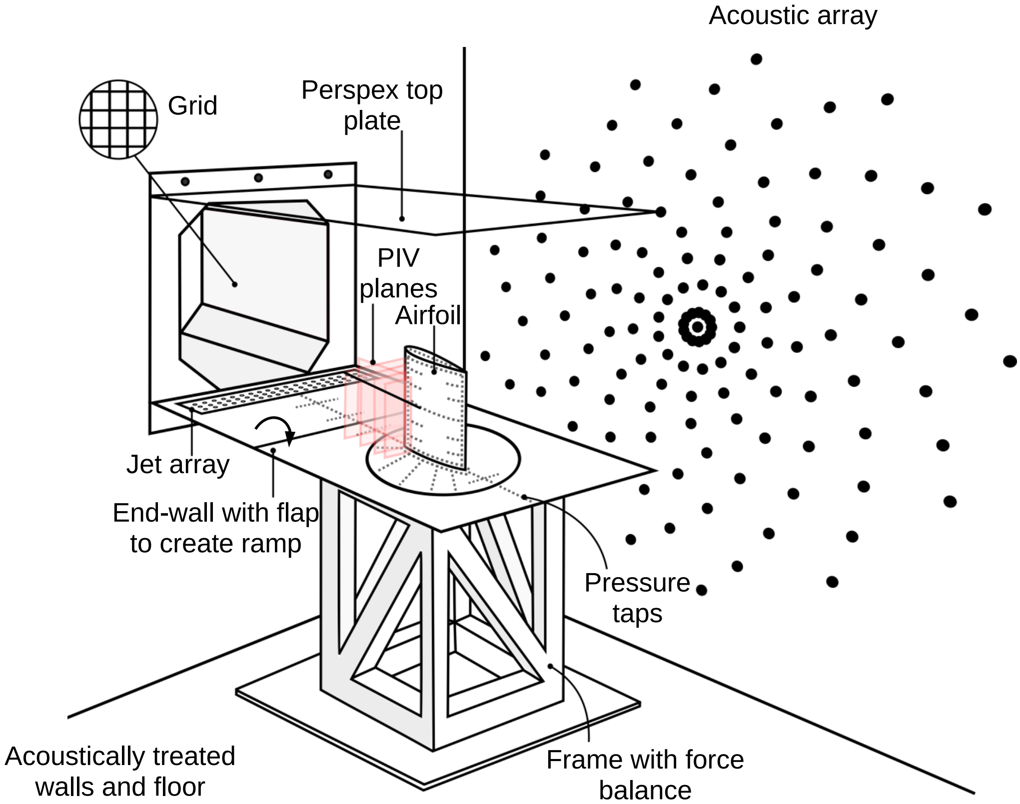

Figure 14: Conceptual sketch of the wall-mounted finite airfoil leading edge noise experiment.

8 CONCLUSIONS

This paper has provided a summary of the aeroacoustic source mechanisms of a wall-mounted finite airfoil. Junction noise due to horseshoe vortex interaction with the airfoil leading edge is a low frequency noise source while at mid-to-high frequencies, the dominant noise sources are airfoil trailing edge noise and the formation of three-dimensional vortex flow near the airfoil trailing edge-tip.

Our research program to date has focused on examining the trailing edge, tip and junction flow regimes of a wall-mounted finite airfoil and their associated noise generation. A semi-empirical prediction method has been developed for the turbulent boundary layer trailing edge noise produced by a three-dimensional airfoil that incorporates tip flow effects. We have also shown that airfoil aspect ratio, camber and thickness alter the local flow conditions on the airfoil surface impacting the trailing edge tonal noise signature in a laminar-transitional flow regime. Noise measurements have been presented to shed light on the nature of tip noise production. Tip noise manifests itself as a broad peak in the airfoil noise spectrum that increases in amplitude with angle of attack. The shape of the airfoil tip influences the tip vortex topology and its associated noise generation. Tip rounding effects can reduce the tip noise level by more than 5 dB at mid-to-high frequencies. Novel tip noise devices that incorporate porosity, serrations and end plates have also been investigated. Finally, mean and fluctuating wall pressure measurements in the vicinity of the junction region have been obtained to elucidate features of the junction flow field. The presence of the airfoil, its aspect ratio and the angle of attack are shown to alter the magnitude and spectral energy of the wall pressure field around the entire airfoil.

Research is needed to understand the leading edge noise generation of a wall-mounted finite airfoil and this will be the focus of our future research program. We have constructed a novel, turbulence and boundary layer-airfoil interaction experiment in the UAT that will allow us to examine leading edge noise in homogenous, isotropic turbulence and anisotropic turbulent boundary layers. This experimental campaign will provide new insight into the leading edge noise generation of a three-dimensional airfoil in complex turbulence.

ACKNOWLEDGEMENTS

The author gratefully acknowledges the support of the Australian Research Council (Project ID: DE150101528; DP200101626) and the Australia-Germany Joint Research Co-operation Scheme (DAAD) (Project ID: 57445107). This paper is largely based on a series of previous papers by the author and colleagues, which are cited. In particular, the author would like to acknowledge Manuj Awasthi, Tingyi Zhang, Yuchen Ding, Con Doolan, Charitha de Silva and Thomas Geyer for their valuable contributions to this body of work.

REFERENCES

Arbey, H. and Bataille, J. (1983). 'Noise generated by airfoil profiles placed in a uniform laminar flow', *Journal of Fluid Mechanics*, 134, pp. 33 – 47.

Awasthi, M., Moreau, D.J. and Doolan, C.J. (2018). 'Flow structure of a low aspect ratio wall-mounted airfoil operating in a low Reynolds number flow', *Experimental Thermal and Fluid Science*, 99, pp. 94 – 116.

Awasthi, M., Rowlands, J., Moreau, D.J. and Doolan, C.J. (2020). 'The effect of aspect ratio on wall pressure fluctuations at a wing-plate junction', *Journal of Fluids Engineering*, 142, 071202.

Brooks, T.F. and Marcolini, M.A. (1986), 'Airfoil Tip Vortex Formation Noise', *AIAA Journal*, 24(2), pp. 246 – 252.

Brooks, T.F., Pope, D., and Marcolini, M. (1989). 'Airfoil Self Noise and Prediction', NASA TR-1218.

Buffo, R.M., Wolf, C.C., Dufhaus, S., Hoernschemeyer, R. and Stumpf, E. (2012). 'Vortex creation and wing-tip geometry dependencies', *30th AIAA Applied Aerodynamics Conference*, AIAA 2021-2770, New Orelans, LA.

Ding, Y., Moreau, D.J., de Silva, C.M. and Doolan, C.J. (2020). 'Experimental investigation of the mean pressure field at airfoil-wall junctions', *Proceedings of the 22nd Australasian Fluid Mechanics Conference*, Brisbane QLD, 6 – 10 December.

Ding, Y., Zhang, T., Geyer, T., de Silva, C., Doolan, C. and Moreau, D. (2021). 'Experimental investigation of the flow characteristics and noise generation at the wing-wall junction', *ASCE Journal of Aerospace Engineering*, 34(5), 04021054.

Ffowcs Williams, J.E. and Hall, L.H. (1970). 'Aerodynamic sound generation by turbulent flow in the vicinity of a scattering half plane', *Journal of Fluid Mechanics*, 40, pp. 657 – 670.

Geyer, T. and Moreau, D. (2021). 'A study of the effect of airfoil thickness on the tonal noise generation of finite, wall-mounted airfoils', *Aerospace Science and Technology*, 115, 106768.

Geyer, T., Moreau, D., Zhang, T., Schneehagen, E. and Ding, Y. (2020). 'Experimental investigation of novel, low-noise turbine blade tip designs', *Proceedings of DAGA 2020*, Hannover Germany, 16 – 19 March.

Giuni, M. and Green, R.B. (2013). 'Vortex formation on squared and rounded tip', *Aerospace Science and Technology*, 29, pp. 191 – 199.

Katz, J., and Plotkin, A., *Low-Speed Aerodynamics*, 2nd ed., Cambridge Univ. Press, Cambridge, England, UK, 2001.

Mathias, D.L., Pye, J.D. and Catwell, B.J. (1998), 'Correlation of wingtip noise with mean flow parameters', *16th AIAA Applied Aerodynamics Conference*, AIAA 98 – 2738, Albuquerque, NM.

Moreau, D.J. and Doolan, C.J. (2016a). 'An experimental study of airfoil tip vortex formation noise', *Proceedings of Acoustics 2016*, Brisbane, Australia, 9 – 11 November.

Moreau D.J. and Doolan, C.J., (2016b). 'Tonal noise production from a wall-mounted finite airfoil', *Journal of* Sound *and Vibration*, 363, pp. 188 – 224.
Moreau, D.J. Doolan, C.J., Alexander, W.N., Meyers, T.W. and Devenport, W.J. (2016). 'Wall-mounted finite airfoil noise production and prediction', *AIAA Journal*, 54(5), pp. 1637 – 1651.
Moreau, D.J., Geyer, T.F., Doolan, C.J. and Sarradj, E. (2018). 'Surface curvature effects on the tonal noise of a wall-mounted finite airfoil', *Journal of the Acoustical Society of America*, 143(6), pp. 3460 – 3473.
Moreau, D.J., Prime, Z., Porteous R., Doolan, C.J. and Valeau, V. (2014). 'Flow-induced noise of a wall-mounted finite airfoil at low-to-moderate Reynolds number', *Journal of Sound and Vibration,* 333(25), pp. 6924 – 6941.
Nash, E.C., Lowson, M.V. and McAlpine, A. (1999). 'Boundary-layer instability noise on aerofoils', *Journal of Fluid Mechanics*, 382, pp. 27–61.
Probsting, S. and Yarusevych, S. (2015). 'Laminar separation bubble development on an airfoil emitting tonal noise', *Journal of Fluid Mechanics*, 780, pp. 167–191.
Schneehagen, E., Geyer, T., Sarradj, E. and Moreau, D. (2021). 'Aeroacoustic noise reduction by application of end plates on wall-mounted finite airfoils', *Experiments in Fluids*, 26, pp. 106 – 106.
Simpson, R.L. (2001). 'Junction Flows', *Annual Review of Fluid Mechanics*, 33, pp. 415 – 443.
Zhang, T., Geyer, T., de Silva, C., Fischer, J., Doolan, C. and Moreau, D. (2021). 'Experimental investigation of tip vortex formation noise produced by wall-mounted finite airfoils', *ASCE Journal of Aerospace Engineering*, 34(6), 04021079.
Zhang, T., Moreau, D.J., Geyer, T., Fischer, J. and Doolan, C.J. (2020a). 'Dataset on tip vortex formation noise produced by wall-mounted finite airfoils with flat and rounded tip geometries', *Data in Brief*, 28, 105058.
Zhang, T., Moreau, D.J., Geyer, T., Fischer, J. and Doolan, C.J. (2020b). 'Dataset on tip vortex formation noise produced by wall-mounted finite airfoils with sinusoidal and porous tip geometries', *Data in Brief*, 30, 105471.